Shedding light on dark sectors with gravitational waves

Nelleke Bunji, Bartosz Fornal, and Kassandra Garcia
Department of Chemistry and Physics, Barry University, Miami Shores, Florida 33161, USA

(Received 30 May 2024; accepted 26 August 2024; published 24 October 2024)

The nature of dark matter remains one of the greatest unsolved mysteries in elementary particle physics. It might well be that the dark matter particle belongs to a dark sector completely secluded or extremely weakly coupled to the visible sector. We demonstrate that gravitational waves arising from first-order phase transitions in the early Universe can be used to look for signatures of dark sector models connected to neutron physics. This introduces a new connection between gravitational-wave physics and nuclear physics experiments. Focusing on two particular extensions of the Standard Model with dark U(1) and SU(2) gauge groups constructed to address the neutron lifetime puzzle, we show how those signatures can be searched for in future gravitational-wave and astrometry experiments.

DOI: 10.1103/PhysRevD.110.075030

I. INTRODUCTION

Elementary particle physics is a unique area of science in the sense that it attempts to answer the most fundamental questions about the Universe and its basic constituents. The currently accepted Standard Model works extremely well and precisely describes interactions of the known particles in the visible Universe. It has withstood experimental tests for the last 50 years since its formulation in the 1970s [1–8], culminating in the discovery of the Higgs particle in 2012 at the Large Hadron Collider [9,10].

Nevertheless, the discovery of dark matter from galactic rotation curves in the 1970s [11] constantly reminds us that this is not the end of the story. Its existence has been confirmed through various other observations, including the cosmic microwave background [12] and gravitational lensing [13]. However, the nature of dark matter remains a puzzle and is certainly one of the most intriguing and crucial questions to answer. We do not even know whether it is an elementary particle or a macroscopic object. The mass of an elementary particle could be anywhere between $\sim 10^{-31}$ GeV (fuzzy dark matter [14,15]) and $\sim 10^{19}$ GeV (WIMPzillas [16,17]), with many well-motivated candidates situated closer to the center of this mass spectrum [18]. If macroscopic, dark matter objects can have masses between $\sim 10^{17}$ GeV (dark quark nuggets [19]) and $\sim 10^{59}$ GeV (primordial black holes [20,21]). Thus far, searches at the Large Hadron Collider, direct-detection experiments (such as XENONnT [22]), and indirect-detection experiments (e.g., Fermi Satellite [23]) have produced only upper limits on the dark matter couplings to the visible sector.

In light of the null dark matter search results, especially for some of the best-motivated candidates such as the weakly interacting massive particles in the $\mathcal{O}(100\ \text{GeV})$ mass regime, one needs to use any theoretical and experimental hints currently available. From a theoretical perspective, it is intriguing that the abundances of dark matter and ordinary matter are of the same order, which suggests that the two sectors might be related and perhaps share a common origin. Theories of asymmetric dark matter are based on this assertion and turn this observation into a prediction for the dark matter mass to be $\mathcal{O}(\text{GeV})$, at the same time explaining the matter-antimatter asymmetry of the Universe [24–29]. This mass range for the dark matter particle has also triggered increased interest on the experimental side, as it was demonstrated that an $\mathcal{O}(1\ \text{GeV})$ dark matter particle might appear in the final state of the new dark decay channel of the neutron, providing a possible explanation of the neutron lifetime anomaly [30] in nuclear physics experiments.

This anomaly arises from the discrepancy between two qualitatively different types of measurements of the neutron lifetime. In the first type of experiments, the bottle method, ultracold neutrons are trapped in a container whose interior is padded with neutron-reflecting material. The container is then emptied at various storage times and the number of remaining neutrons is determined using a proportional counter. An exponential decay curve is then fitted to those data points and the neutron lifetime is extracted from the fit. The average of the bottle neutron lifetime experiments [31–38] is $\tau_n^{\text{bottle}} = 878.4 \pm 0.5$ s. In the second type of measurements, the beam method, a beam of cold neutrons passes through a quasi-Penning trap, which collects and counts the protons from neutron

decays, enabling the determination of the neutron decay rate involving protons in the final state. Estimating the number of neutrons in the beam, the neutron lifetime is calculated by dividing this number by the rate of decay to protons. The average of the beam neutron lifetime measurements [39–42] is $\tau_n^{\text{beam}} = 888.0 \pm 2.0$ s, which is four standard deviations away from the bottle result.

Although this mismatch may be due to some unknown systematic errors, it was demonstrated in [30] that a neutron decay channel into dark-sector particles can account for this. In particular, if the branching fraction for neutron beta decay is 99%, whereas the remaining 1% of decays involve particles from a dark sector with no protons in the final state, the two experimental results are reconciled. This proposal for the existence of a neutron dark decay channel was followed by a plethora of theoretical works [43–57] and experimental efforts and proposals [58–66]; for a review, see [67]. In this paper, we complement this literature by analyzing the possible gravitational-wave signatures from UV-complete theories constructed for the neutron dark decay channel, focusing on the models constructed in [48,54].

Recently, a novel and very promising avenue of probing particle physics models has emerged with the first confirmed detection of gravitational waves by the Laser Interferometer Gravitational-Wave Observatory (LIGO) [68]. Although this signal and some $\mathcal{O}(100)$ subsequent events arose from mergers of black holes and/or neutron stars, gravitational waves could have been produced in the early Universe as well. Among the most spectacular hypothetical processes occurring shortly after the big bang and leading to a potentially measurable stochastic gravitational-wave background today are first-order phase transitions [69], cosmic strings [70,71], domain walls [72], and inflation [73].

First-order phase transitions are especially interesting, since they strongly depend on the particle-physics details. They are triggered when the effective potential develops a deeper minimum (true vacuum) at a nonzero field value separated from the high-temperature minimum (false vacuum) by a potential barrier. When a given point in the Universe transitions from the false vacuum to the true one, this corresponds to a nucleation of an expanding bubble of true vacuum. Such a process can happen at multiple points in space, eventually causing the entire Universe to transition to the true vacuum state. During the bubble nucleation and expansion, gravitational waves are emitted from sound waves in the primordial plasma, bubble collisions, and turbulence. There is vast literature on the subject analyzing a plethora of particle physics models, including new electroweak-scale physics [74–82], dark sectors [83–90], axions [91–94], unification [95–98], conformal invariance [99,100], supersymmetry [101,102], left-right symmetry [103,104], neutrino mass models [105–108], baryon and lepton number violation [109–111], flavor physics [112,113], and leptogenesis [114,115]. For a review of the subject, see, e.g., [116], and for the LIGO observing run O3 constraints on particle physics models, see [117].

The reach of gravitational-wave observations will improve considerably with future detectors, such as the Laser Interferometer Space Antenna [118], Cosmic Explorer [119], Big Bang Observer [120], Einstein Telescope [121], and DECIGO [122]. In addition to gravitational-wave measurements using interferometers, there are several existing and upcoming observational efforts to detect gravitational waves through their effect on pulsar timing arrays, which are sensitive to much lower frequencies. These include NANOGrav [123], PPTA [124], EPTA [125], IPTA [126], and SKA [127]. It is worth noting that NANOGrav recently detected a stochastic gravitational-wave signal in the $\sim 10^{-8}$ Hz frequency region [128].

The aim of this paper is to demonstrate that gravitational-wave experiments grant access to a yet unexplored parameter space of models relevant for nuclear physics. For concreteness, we focus on two models constructed for neutron dark decay and describe them in Secs. II and III, with both of them containing a dark sector, but only the second one accommodating dark matter. Section IV analyzes the first-order phase transition in each model. Finally, in Sec. V we derive the expected gravitational-wave signatures and comment on their relation to the recent NANOGrav signal. Our findings are summarized in Sec. VI.

II. MODEL 1

The first model we consider is based on the symmetry [48]

$$\mathrm{SU}(3)_c \times \mathrm{SU}(2)_L \times \mathrm{U}(1)_Y \times \mathrm{U}(1)_D, \tag{1}$$

with the dark $\mathrm{U}(1)_D$ gauge group spontaneously broken at the energy scale $\mathcal{O}(60\ \mathrm{MeV})$. The neutron dark decay channel proposed in [48] is $n \to \chi A'$, where χ is a dark fermion and A' is a dark photon.

In this section, we complement this analysis by considering, within the framework of this model, the neutron dark decay channel $n \to \chi\phi$, where ϕ is the scalar responsible for $\mathrm{U}(1)_D$ symmetry breaking. As will be shown in Sec. V, this scenario leads to a measurable gravitational-wave signal.

A. Particle content and Lagrangian

The theory extends the Standard Model by introducing the following new fields:

(1) Complex scalar $\phi = (1, 1, 0, 1)$ with baryon number $B_\phi = 0$, responsible for the breaking of $\mathrm{U}(1)_D$.
(2) Dirac fermion $\chi = (1, 1, 0, 1)$ carrying $B_\chi = 1$, a dark particle and product of neutron dark decay.

(3) Dark photon A' from $\mathrm{U}(1)_D$ breaking, which alleviates neutron star constraints.
(4) Two complex scalars triplets $\Phi_1 = (3, 1, \frac{1}{3}, -1)$ and $\Phi_2 = (3, 1, \frac{1}{3}, 0)$, with $B_\Phi = -2/3$, providing the interactions for the neutron dark decay to be triggered.

The beyond-the-Standard-Model Lagrangian terms relevant for neutron dark decay and generating masses for χ, A', ϕ are

$$\begin{aligned}\mathcal{L} \supset\ & |D_\mu \phi|^2 + \lambda\left[|\phi|^2 - \left(\frac{v_D}{\sqrt{2}}\right)^2\right]^2 + \bar{\chi}(i\not{D} - m_\chi)\chi \\ & + \lambda_1 \bar{d}^i P_L \chi \Phi_{1i} + \lambda_2 \epsilon^{ijk} \bar{u}_i^c P_R d_j \Phi_{2k} \\ & + \mu\, \Phi_{1i} \Phi_2^{*i} \phi - \frac{1}{4} F'_{\mu\nu} F'^{\mu\nu} - \frac{\delta}{2} F_{\mu\nu} F'^{\mu\nu}, \end{aligned} \tag{2}$$

where the covariant derivative is $D_\mu = \partial_\mu - i g_D A'_\mu$ and i, j, k are color indices. A nonzero δ parameter allows for a kinetic mixing between A' and the photon, leading to the decay channel $A' \to e^+ e^-$.

Upon spontaneous breaking of the $\mathrm{U}(1)_D$ gauge symmetry when ϕ develops the vacuum expectation value $\langle\phi\rangle = v_D/\sqrt{2}$, the dark photon and scalar ϕ acquire the masses

$$\begin{aligned} m_{A'} &= \frac{g_D v_D}{\sqrt{2}}, \\ m_\phi &= \sqrt{2\lambda}\, v_D. \end{aligned} \tag{3}$$

We assume that the masses of the scalars Φ_1 and Φ_2 are generated at a higher scale and are much larger than the masses of χ, A', ϕ, so they can be integrated out.

B. Low-energy effective theory

Below the mass scale of Φ_1 and Φ_2, an effective coupling of the dark particle χ to the neutron and ϕ is generated,

$$\mathcal{L}_{n\chi\phi} = \frac{\varepsilon\sqrt{2}}{v_D} \bar{n} P_L \chi \phi, \tag{4}$$

where

$$\varepsilon = \frac{\beta \mu v_D \lambda_1 \lambda_2}{m_{\Phi_1}^2 m_{\Phi_2}^2}, \tag{5}$$

with β being the matching coefficient determined from a lattice calculation, $\beta = 0.0144(3)(21)$ GeV^3 [129]. Therefore, after $\mathrm{U}(1)_D$ breaking, the nonstandard contribution to the effective Lagrangian at the nuclear level is

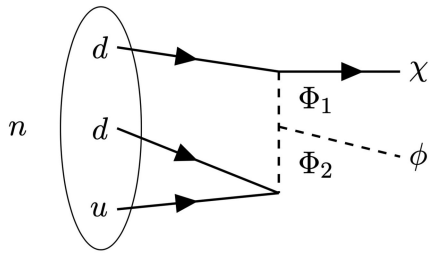

FIG. 1. Possible neutron dark decay channel $n \to \chi\phi$ in the dark $\mathrm{U}(1)_D$ model [48] and in the dark $\mathrm{SU}(2)_D$ model [54].

$$\begin{aligned}\mathcal{L}_{\text{eff}} =\ & \bar{\chi}(i\not{D} - m_\chi)\chi + \varepsilon(\bar{n}\chi + \bar{\chi}n) - \frac{1}{2} m_{A'}^2 A'^\mu A'_\mu \\ & - \frac{1}{4} F'_{\mu\nu} F'^{\mu\nu} - \frac{\delta}{2} F_{\mu\nu} F'^{\mu\nu} + \frac{\varepsilon\sqrt{2}}{v_D}(\bar{n}\chi + \bar{\chi}n)\phi. \end{aligned} \tag{6}$$

Depending on the details of the spectrum of the theory, these interactions can lead to neutron dark decay. The focus of [48] was on $n \to \chi A'$, which would yield a rate of

$$\Gamma(n \to \chi A') = \frac{g_D^2 \varepsilon^2}{8\pi} \frac{(m_n - m_\chi)}{m_{A'}^2} \left(1 - \frac{m_{A'}^2}{(m_n - m_\chi)^2}\right)^{\frac{3}{2}}. \tag{7}$$

However, the other possibility within this model, not analyzed in [48], is the decay channel $n \to \chi\phi$ (see Fig. 1). We find that the corresponding neutron dark decay rate is

$$\begin{aligned}\Gamma(n \to \chi\phi) =\ & \frac{\varepsilon^2}{8\pi v_D^2 m_n} \sqrt{(m_n - m_\chi)^2 - m_\phi^2} \\ & \times \sqrt{(m_n + m_\chi)^2 - m_\phi^2}. \end{aligned} \tag{8}$$

As discussed below, there exists a range of parameter values for which this decay rate corresponds to a neutron decay branching fraction of 1%, which is needed to explain the neutron lifetime discrepancy, while remaining consistent with all experimental and observational constraints.

C. Phenomenology

Given the complexity of the relations between parameters in the model, we focus on particular benchmark scenarios with fixed masses for χ and ϕ. The constraints arise from various cosmological and astrophysical observations, but they are not very sensitive to the precise choices of the particle masses.

1. Neutron dark decay

To prevent neutrons in stable nuclei from undergoing dark decays, one requires [60]

$$937.993\ \text{MeV} < m_\chi + m_\phi < 939.565\ \text{MeV}, \tag{9}$$

where the lower bound is slightly higher than in the original proposal [30] due to taking into account a rapid disintegration of excited ^{8}Be into two α particles. The dark particle χ is assumed to be Dirac to avoid bounds from dinucleon decay searches. In addition, when ϕ develops a vacuum expectation value, the interaction in Eq. (4) produces the mixing term $\bar{n}\chi$, which could also lead to the decay of stable nuclei. To kinematically forbid such decays, we require

$$m_\chi > 937.993 \text{ MeV}. \tag{10}$$

One of the benchmark points (A) we consider is

$$m_\chi = 938 \text{ MeV}, \qquad m_\phi = 0.85 \text{ MeV}, \qquad m_{A'} = 10 \text{ MeV}. \tag{11}$$

In order to resolve the neutron lifetime discrepancy through a 1% branching fraction for the dark decay [30], one needs $\Gamma(n \to \chi\phi) \approx 7 \times 10^{-30}$ GeV. For benchmark (A), this is equivalent to having

$$\varepsilon \approx 1.6 \times 10^{-11} \text{ MeV}. \tag{12}$$

2. Neutron stars

Constraints from observed neutron star masses [43–45] on the models originally proposed in [30] are alleviated by self-interactions in the dark sector mediated by the dark photon. In particular, the resulting repulsive interaction between χ and the neutrons make the neutron star equation of state stiffer. To account for masses of $2M_\odot$, i.e., the largest neutron star masses observed, it is sufficient to require [48]

$$\frac{v_D}{\sqrt{2}} = \frac{m_{A'}}{g_D} \lesssim (45\text{–}60) \text{ MeV}, \tag{13}$$

depending on the assumed nuclear star equation of state. In our analysis, we fulfill Eq. (13) by setting $v_D = 60$ MeV.

3. Cosmology

Further constraints arise from big bang nucleosynthesis, measurements of the cosmic microwave background, and supernova observations. These bounds strongly disfavor a dark photon A' with mass less than $2m_e$. As shown in [48], for $m_{A'} = 1.35$ MeV the allowed range for the parameter δ is limited to $2 \times 10^{-11} < \delta < 2 \times 10^{-9}$, while the dark gauge coupling $g_D > 0.07$. These bounds are fairly independent of the value of $m_{A'}$ as long as $m_{A'} > 2m_e$.

In the scenario we consider, i.e., $n \to \chi\phi$, the dark photon mass does not need to be small. Increasing $m_{A'}$ loosens the cosmological and astrophysical bounds on the model. In addition, we are not considering the case when the dark photon or the dark scalar are the dark matter, which eliminates direct and indirect dark matter detection bounds.

Furthermore, the case of a heavier dark photon is preferred for the gravitational-wave signals. Based on Eq. (3), the ratio of the dark photon mass and dark scalar mass is

$$\frac{m_{A'}}{m_\phi} = \frac{g_D}{2\sqrt{\lambda}}, \tag{14}$$

while gravitational waves from first-order phase transitions (as discussed in Sec. V) provide the strongest signals when $g_D/(2\sqrt{\lambda}) > \mathcal{O}(1)$, which corresponds precisely to the case of a heavier dark photon.

We also note that in the gravitational-wave analysis of the model, we remain general and go beyond the parameter space allowing for a neutron dark decay channel, e.g., we also consider ϕ and A' masses in the multi-MeV range.

III. MODEL 2

We now turn to the model based on the gauge group [54]

$$\text{SU}(3)_c \times \text{SU}(2)_L \times \text{U}(1)_Y \times \text{SU}(2)_D, \tag{15}$$

where $\text{SU}(2)_D$ is broken at energies $\mathcal{O}(60 \text{ MeV})$. There are three scenarios for the neutron dark decay proposed in [54], but we focus on $n \to \chi\phi$, where χ is a dark fermion and ϕ is the scalar responsible for $\text{SU}(2)_D$ breaking. In Sec. V we will demonstrate that this scenario can be probed with gravitational waves and discuss how this case differs from the Abelian model described in Sec. II.

In its structure, Model 2 is very similar to Model 1, but with three differences:

(1) The complex scalar $\Phi = (1, 1, 0, 2)$ responsible for the breaking of $\text{SU}(2)_D$ is a dark doublet,

$$\Phi = \begin{pmatrix} \frac{1}{\sqrt{2}}(G_1 + iG_2) \\ \frac{\phi + v_D}{\sqrt{2}} + iG_3 \end{pmatrix}. \tag{16}$$

(2) Upon symmetry breaking, instead of one dark photon, there are three dark W'^a gauge bosons ($a = 1, 2, 3$).

(3) The complex scalar triplet Φ_1 is now an $SU(2)_D$ doublet: $\Phi_1 = (3, 1, \frac{1}{3}, 2)$.

The Lagrangian takes the form

$$\begin{aligned}\mathcal{L} \supset\ & |D_\mu \Phi|^2 + \lambda\left[|\Phi|^2 - \left(\frac{v_D}{\sqrt{2}}\right)^2\right]^2 + \bar{\chi}(i\not{D} - m_\chi)\chi \\ & + [\lambda_1 \bar{d}^i P_L \chi \Phi_{1i} + \lambda_2 \epsilon^{ijk} \bar{u}_i^c P_R d_j \Phi_{2k} \\ & + \mu\, \Phi_{1i}\Phi_2^{*i}\Phi + \text{H.c.}] - \frac{1}{4} W'^a_{\mu\nu} W'^{a,\mu\nu} \\ & + [c_1 \text{Tr}(\Phi^\dagger \tau^a \Phi W'^a_{\mu\nu} F^{\mu\nu}) + c_2 \text{Tr}(\Phi^\dagger \tau^a \Phi W'^a_{\mu\nu} \tilde{F}^{\mu\nu}) \\ & + c_3 \text{Tr}(\Phi^\dagger \tau^a \Phi \tilde{W}'^a_{\mu\nu} F^{\mu\nu}) + \text{H.c.}], \end{aligned} \tag{17}$$

where the covariant derivative is $D_\mu = \partial_\mu - i g_D \tau^a W^a_\mu$, $W'^a_{\mu\nu}$ is the $SU(2)_D$ field-strength tensor, and its dual is given by $\tilde{W}'^a_{\mu\nu} = \epsilon_{\mu\nu\alpha\beta} W'^{a,\alpha\beta}$.

Upon spontaneous breaking of $SU(2)_D$ when Φ develops its vacuum expectation value,

$$\langle \Phi \rangle = \frac{1}{\sqrt{2}} \begin{pmatrix} 0 \\ v_D \end{pmatrix}, \tag{18}$$

the dark W'^a gauge bosons and the radial component of the scalar Φ acquire the following masses:

$$\begin{aligned} m_{W'} &= \frac{g_D v_D}{\sqrt{2}}, \\ m_\phi &= \sqrt{2\lambda}\, v_D. \end{aligned} \tag{19}$$

Assuming again that the masses of the scalars Φ_1 and Φ_2 are generated at a higher scale than v_D, and upon integrating them out, one arrives at a similar low-energy effective theory as for Model 1 in Eq. (6), but with the dark photon terms replaced by those containing the W'^a gauge boson fields.

Depending on the masses of the particles, the possible dark decay channels for the neutron are $n \to \chi W'$ and $n \to \chi\phi$. For similar reasons as before, i.e., to have a scenario with measurable gravitational-wave signals, we assume

$$\frac{m_{W'}}{m_\phi} = \frac{g_D}{2\sqrt{\lambda}} > \mathcal{O}(1). \tag{20}$$

Consequentially, we focus again on the $n \to \chi\phi$ dark decay channel (see Fig. 1), since it is realized when the condition in Eq. (20) is fulfilled. The formula for the decay rate is identical to that in Eq. (8), and there is again a range of possible parameter values for which this decay rate yields a neutron dark decay branching fraction of 1%.

We consider the benchmark point (A)′, similar to (A) for Model 1, but with the dark photon replaced by W',

$$m_\chi = 938\ \text{MeV}, \qquad m_\phi = 0.85\ \text{MeV}, \qquad m_{W'} = 8\ \text{MeV}, \tag{21}$$

which results in the same value of ε as that in Eq. (12). Neutron star constraints translate to

$$\frac{v_D}{\sqrt{2}} = \frac{m_{W'}}{g_D} \lesssim (45\text{–}60)\ \text{MeV}, \tag{22}$$

and we again take $v_D = 60$ MeV.

It was argued in [54], in agreement with [48], that χ cannot be the sole component of dark matter. At the same time, it was demonstrated that the dark matter can be made up of a combination of ϕ and W'^a, or just the W'^a, depending on the region of parameter space. These dark matter particles would be produced via the freeze-in mechanism [54].

Constraints arising from cosmology, astrophysics (other than neutron stars), and dark matter direct detection are all less severe than the requirement of the correct dark matter relic density. In particular, the big bang nucleosynthesis bounds are mild as long as $m_{W'} > 2m_e$, the cross section for indirect dark matter detection is extremely small and does not provide any noteworthy bound, and the direct dark matter detection constraints are even less constraining.

The cosmological and astrophysical bounds on the model are not very sensitive to m_ϕ, leading to similar exclusion regions for our benchmark point as in scenario **C** in [54], i.e., for the dark gauge coupling $g_D > 0.05$ and the coefficient for the first trace term in Eq. (17) $c_1 < (10^{-14}, 10^{-9})\ \text{GeV}^{-2}$ as g_D changes in the range (0.05,1).

IV. FIRST-ORDER PHASE TRANSITION

We now investigate the possibility of a first-order phase transition being triggered by $U(1)_D$ breaking in Model 1 and $SU(2)_D$ breaking in Model 2 around the scale $\mathcal{O}(60\ \text{MeV})$. We first calculate the effective potential for both models, and then determine the effective action for the bounce solution. This is then used to find the phase transition parameters α, $\tilde{\beta}$, and T_*, ultimately leading to a prediction for the gravitational-wave signal, as derived in Sec. V.

A. Effective potential

The effective potential consists of three parts: the tree-level $V_{\text{tree}}(\varphi)$, the one-loop Coleman-Weinberg correction $V_{\text{loop}}(\varphi)$, and the finite-temperature contribution $V_{\text{temp}}(\varphi, T)$, where φ is the background field,

$$V_{\text{eff}}(\varphi, T) = V_{\text{tree}}(\varphi) + V_{\text{loop}}(\varphi) + V_{\text{temp}}(\varphi, T). \tag{23}$$

Plugging into the formula for the tree-level potential the value of m_ϕ obtained by minimizing the potential, one arrives at

$$V_{\text{tree}}(\varphi) = -\frac{1}{2}\lambda v_D^2\varphi^2 + \frac{1}{4}\lambda\varphi^4. \tag{24}$$

To determine the one-loop contribution, we implement the cutoff regularization scheme and choose the minimum of the potential at zero temperature and the mass of ϕ to be equal to their tree-level values. This leads to [130]

$$V_{\text{loop}}(\varphi) = \sum_i \frac{n_i}{(8\pi)^2}\left\{m_i^4(\varphi)\left[\log\left(\frac{m_i^2(\varphi)}{m_i^2(v_D)}\right) - \frac{3}{2}\right] + 2m_i^2(\varphi)m_i^2(v_D)\right\}, \tag{25}$$

where the sum is over all particles charged under $\mathrm{U}(1)_D$ [$\mathrm{SU}(2)_D$], including Goldstone bosons, n_i is the number of degrees of freedom for a given particle species, and m_i are the background field-dependent masses [with the substitution $m_\xi(v_D) \to m_\phi(v_D)$ for the Goldstones].

We find that the background field-dependent masses for the $\mathrm{U}(1)_D$ charged particles in Model 1, i.e., the dark photon A', the scalar ϕ, and the Goldstone boson ξ, are

$$m_{A'}(\varphi) = g_D\varphi, \qquad m_\phi(\varphi) = \sqrt{\lambda(3\varphi^2 - v_D^2)}, \qquad m_\xi(\varphi) = \sqrt{\lambda(\varphi^2 - v_D^2)}, \tag{26}$$

with $n_{A'} = 3$ and $n_\phi = n_\xi = 1$.

In the case of Model 2, the $\mathrm{SU}(2)_D$ charged particles, i.e., the dark gauge bosons W'^a, the scalar ϕ, and the Goldstone bosons ξ^a, have the same background field-dependent masses and number of degrees of freedom as the dark photon, scalar, and Goldstone boson in Model 1, respectively. However, the difference is that there are three W'^a gauge bosons and three Goldstone bosons in the summation.

The temperature-dependent part of the effective potential is given by [131]

$$V_{\text{temp}}(\varphi, T) = \frac{T^4}{2\pi^2}\sum_i n_i \int_0^\infty dx\, x^2 \log\left[1 \mp e^{-\sqrt{x^2 + \frac{m_i^2(\varphi)}{T^2}}}\right] + \frac{T}{12\pi}\sum_k n'_k\left\{m_k^3(\varphi) - [m_k^2(\varphi) + \Pi_k(T)]^{3/2}\right\}. \tag{27}$$

The first part of this expression (sum includes all particles) corresponds to one-loop diagrams, whereas the second part (sum includes only bosons) comes from daisy diagrams, with only longitudinal degrees of freedom for vector bosons involved. The thermal masses $\Pi_k(T)$ are calculated using the formalism presented, e.g., in [132]. Assuming $\lambda \ll 1$, which is fulfilled for the parameter space considered, we obtain the results below.

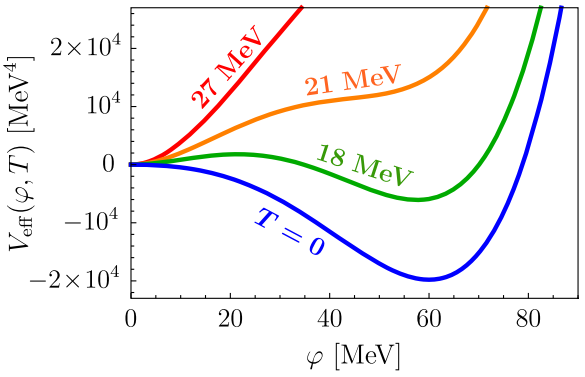

FIG. 2. Effective potential for the $\mathrm{U}(1)_D$ model assuming $g_D = 0.8$, $v_D = 60$ MeV, and $\lambda = 0.01$, plotted for several temperatures.

The thermal masses for the dark photon A', scalar ϕ, and Goldstone boson in Model 1 are

$$\Pi_{A'}(T) = \frac{1}{3}g_D^2T^2, \qquad \Pi_\phi(T) = \Pi_\xi(T) = \frac{1}{4}g_D^2T^2. \tag{28}$$

The values for n_i are the same as in the zero-temperature calculation, whereas $n'_{A'} = 1$ and $n'_\phi = n'_\xi = 1$.

In the $\mathrm{SU}(2)_D$ scenario of Model 2, the thermal masses are

$$\Pi_{W'}(T) = \frac{5}{6}g_D^2T^2, \qquad \Pi_\phi(T) = \Pi_\xi(T) = \frac{3}{4}g_D^2T^2. \tag{29}$$

In this case, $n_{W'} = 3$, $n'_{W'} = 1$, $n_\phi = n_\xi = n'_\phi = n'_\xi = 1$, and there are again three W'^a and three ξ^a fields.

The effective potential for Model 1, assuming $g_D = 0.8$, $v_D = 60$ MeV, $\lambda = 0.01$, and several values of the temperature, is plotted in Fig. 2. As the temperature drops, a new true vacuum at $\varphi \neq 0$ appears with lower energy density than the $\varphi = 0$ false vacuum. The two vacua are separated by a potential barrier, which may result in a first-order phase transition triggering bubble nucleation.

B. Bubble nucleation

The transition from the false vacuum to the true vacuum is initiated when the temperature drops below the nucleation temperature T_*. When this happens, bubbles of true vacuum are nucleated in various parts of the Universe. The nucleation temperature is calculated by comparing the bubble nucleation rate $\Gamma(T)$ with the Hubble expansion rate, since only when the two are comparable will the nucleation be efficient enough to continue. We are therefore looking for a solution to

$$\Gamma(T_*) \sim H(T_*)^4, \tag{30}$$

with the nucleation rate [133]

$$\Gamma(T) \approx \left(\frac{\mathcal{S}(T)}{2\pi T}\right)^{\frac{3}{2}} T^4 \exp\left(-\frac{\mathcal{S}(T)}{T}\right). \tag{31}$$

Here $\mathcal{S}(T)$ is the Euclidean action,

$$\mathcal{S}(T) = 4\pi \int dr\, r^2 \left[\frac{1}{2}\left(\frac{d\varphi_b}{dr}\right)^2 + V_{\text{eff}}(\varphi_b, T)\right], \tag{32}$$

where $\varphi_b(r)$ is the bounce solution determining the profile of the expanding bubble, i.e., the solution of the equation

$$\frac{d^2\varphi}{dr^2} + \frac{2}{r}\frac{d\varphi}{dr} - \frac{dV_{\text{eff}}(\varphi, T)}{d\varphi} = 0 \tag{33}$$

subject to the boundary conditions

$$\left.\frac{d\varphi}{dr}\right|_{r=0} = 0, \qquad \varphi(\infty) = \varphi_{\text{false}}. \tag{34}$$

Using Eqs. (30) and (31), the nucleation temperature T_* is then determined by solving

$$\frac{\mathcal{S}(T_*)}{T_*} \approx 4\log\left[\frac{M_{\text{Pl}}}{T_*}\right] - 2\log\left[\frac{4\pi^3 g_*}{45}\left(\frac{2\pi T_*}{\mathcal{S}(T_*)}\right)^{\frac{3}{4}}\right], \tag{35}$$

where M_{Pl} is the Planck mass.

C. Phase transition parameters

After computing the nucleation temperature, the parameter α describing the phase transition strength is determined from

$$\alpha = \left.\frac{\rho_{\text{vac}}(T)}{\rho_{\text{rad}}(T)}\right|_{T=T_*}, \tag{36}$$

i.e., the offset between the two vacua's energy densities

$$\rho_{\text{vac}}(T) = V_{\text{eff}}(\varphi_{\text{false}}, T) - V_{\text{eff}}(\varphi_{\text{true}}, T) - T\frac{\partial}{\partial T}\left[V_{\text{eff}}(\varphi_{\text{false}}, T) - V_{\text{eff}}(\varphi_{\text{true}}, T)\right] \tag{37}$$

divided by the energy density of radiation

$$\rho_{\text{rad}}(T) = \frac{\pi^2}{30} g_* T^4. \tag{38}$$

The parameter $\tilde{\beta}$, determining the inverse of the duration of the phase transition, can be calculated via

$$\tilde{\beta} = T_* \frac{d}{dT}\left(\frac{\mathcal{S}(T)}{T}\right)\bigg|_{T=T_*}. \tag{39}$$

V. GRAVITATIONAL-WAVE SIGNAL

When bubbles of true vacuum are nucleated and violently expand, the combined effect of collisions between their walls, sound shock waves in the plasma, and magnetohydrodynamic turbulence gives rise to gravitational waves, which propagate through the Universe and would reach us today in the form of a stochastic gravitational-wave background.

The shape of its spectrum has been successfully modeled through numerical simulations. It depends on four parameters: v_w, the speed of the bubble wall, which we take to be the speed of light (see [134,135] for other choices); T_*, the nucleation temperature; α, the strength of the phase transition; and $\tilde{\beta}$, the inverse of its duration. Their values are determined by the shape of the effective potential and thus are governed by the details of the particle physics at play in the early Universe. This establishes a connection between the Lagrangian parameters of a given particle physics model and the spectrum of the resulting gravitational waves.

The contribution from sound waves is given by the empirical formula [135,136]

$$h^2\Omega_s(f) \approx \frac{1.9\times 10^{-5}}{\tilde{\beta}}\left(\frac{100}{g_*}\right)^{\frac{1}{3}}\left(\frac{\alpha\kappa_s}{\alpha+1}\right)^2 \frac{(f/f_s)^3\Upsilon}{[1+0.75(f/f_s)^2]^{\frac{7}{2}}}, \tag{40}$$

where

$$\kappa_s = \frac{\alpha}{0.73 + 0.083\sqrt{\alpha} + \alpha},$$
$$f_s = (1.9\times 10^{-9}\ \text{Hz})\left(\frac{T_*}{10\ \text{MeV}}\right)\left(\frac{g_*}{100}\right)^{\frac{1}{6}}\tilde{\beta},$$
$$\Upsilon = 1 - \frac{1}{\sqrt{1 + \frac{8\pi^{1/3}}{\tilde{\beta}}\sqrt{\frac{\alpha+1}{3\alpha\kappa_s}}}} \tag{41}$$

are, respectively, the fraction of the latent heat transformed into the bulk motion of the plasma [134], the peak frequency for $h^2\Omega_s$, and the suppression factor [137,138].

The contribution to the gravitational-wave spectrum from bubble-wall collisions is [69,135,139]

$$h^2\Omega_c(f) \approx \frac{4.9\times 10^{-6}}{\tilde{\beta}^2}\left(\frac{\alpha\kappa_c}{\alpha+1}\right)^2\left(\frac{100}{g_*}\right)^{\frac{1}{3}} \frac{(f/f_c)^{2.8}}{1+2.8(f/f_c)^{3.8}}, \tag{42}$$

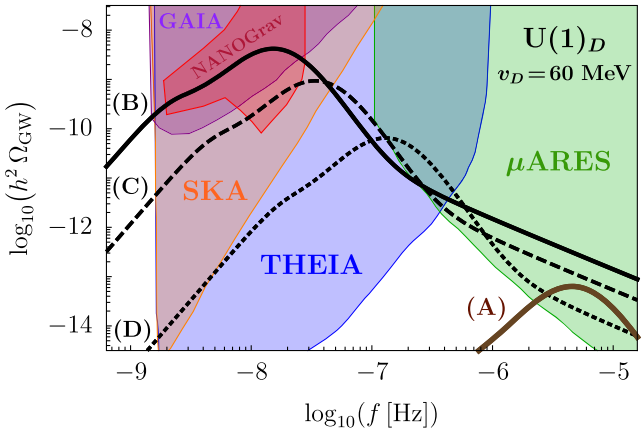

FIG. 3. Gravitational-wave signatures of a first-order phase transition in the dark $\mathrm{U}(1)_D$ model [48] assuming $v_D = 60$ MeV, plotted for the Lagrangian parameters (g_D, λ) specified in Table I. The shaded regions correspond to the reach of future gravitational-wave and astrometry experiments: SKA [127] (orange), μARES [143] (green), THEIA [144] (blue), GAIA [145,146] (purple), and the 15-year NANOGrav signal region [128] (red).

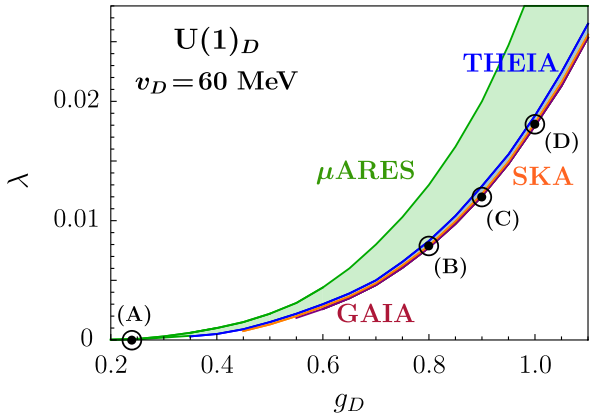

FIG. 4. Parameter space (g_D, λ) for which the gravitational-wave signal from a first-order phase transition in the dark $\mathrm{U}(1)_D$ model is discoverable with a signal-to-noise ratio of at least 5 after the mission lifetime is completed for each of the experiments: GAIA (purple), THEIA (blue), SKA (orange), and μARES (green). The circled dots correspond to the signal curves in Fig. 3.

where

$$\kappa_c = \frac{\frac{4}{27}\sqrt{\frac{3}{2}\alpha} + 0.72\alpha}{1 + 0.72\alpha},$$
$$f_c = (3.7 \times 10^{-10}\ \mathrm{Hz})\left(\frac{T_*}{10\ \mathrm{MeV}}\right)\left(\frac{g_*}{100}\right)^{\frac{1}{6}}\tilde{\beta} \quad (43)$$

are the fraction of the latent heat deposited into the bubble front [140] and the peak frequency for $h^2\Omega_c$, respectively.

Last, the contribution from magnetohydrodynamic turbulence is given by [141,142]

$$h^2\Omega_t(f) \approx \frac{3.4 \times 10^{-4}}{\tilde{\beta}}\left(\frac{\alpha\epsilon\kappa_s}{\alpha+1}\right)^{\frac{3}{2}} \times \left(\frac{100}{g_*}\right)^{\frac{1}{3}} \frac{(f/f_t)^3}{(1 + 8\pi f/h_*)(1 + f/f_t)^{11/3}}, \quad (44)$$

in which ϵ is the turbulence suppression parameter, which we set to $\epsilon = 0.05$ following [135], and where

$$f_t = (2.7 \times 10^{-9}\ \mathrm{Hz})\left(\frac{T_*}{10\ \mathrm{MeV}}\right)\left(\frac{g_*}{100}\right)^{\frac{1}{6}}\tilde{\beta},$$
$$h_* = (1.7 \times 10^{-9}\ \mathrm{Hz})\left(\frac{T_*}{10\ \mathrm{MeV}}\right)\left(\frac{g_*}{100}\right)^{\frac{1}{6}} \quad (45)$$

are the peak frequency and inverse Hubble time at gravitational-wave production redshifted to today [135], respectively.

The combined stochastic gravitational-wave spectrum from phase transitions is obtained by adding the three contributions,

$$h^2\Omega_{\rm GW}(f) = h^2\Omega_s(f) + h^2\Omega_c(f) + h^2\Omega_t(f). \quad (46)$$

Upon performing the procedure outlined in Sec. IV for various values of the gauge coupling g_D and the quartic coupling λ within the dark $\mathrm{U}(1)_D$ model, keeping the vacuum expectation value fixed at $v_D = 60$ MeV, and using the empirical expressions in Eqs. (40)–(46), we arrive at the representative gravitational-wave signals shown in Fig. 3. The curves correspond to the four choices of the Lagrangian parameters: $(g_D, \lambda) = (0.24, 0.0001)$ [brown solid line, curve (A)], $(g_D, \lambda) = (0.8, 0.008)$ [black solid line, curve (B)], $(g_D, \lambda) = (0.9, 0.012)$ [long-dashed line, curve (C)], and $(g_D, \lambda) = (1.0, 0.018)$ [short-dashed line, curve (D)]. We overplot the anticipated sensitivities of future experiments: the pulsar timing array SKA [127], the space-based interferometer μARES [143], and the astrometry

TABLE I. Correspondence between the Lagrangian parameters (g_D, λ) of the $\mathrm{U}(1)_D$ model ($v_D = 60$ MeV) and the resulting phase transition parameters $(\alpha, \tilde{\beta}, T_*)$ for the signals plotted in Fig. 3.

	$\mathrm{U}(1)_D$ model parameters				Transition parameters		
Signal	g_D	λ	m_ϕ [MeV]	$m_{A'}$ [MeV]	α	$\tilde{\beta}$	T_* [MeV]
(A)	0.24	0.0001	0.85	10	0.7	6600	3.6
(B)	0.8	0.008	7.6	34	4.3	20	4.0
(C)	0.9	0.012	9.3	38	1.0	30	5.9
(D)	1.0	0.018	11.4	42	0.4	80	8.5

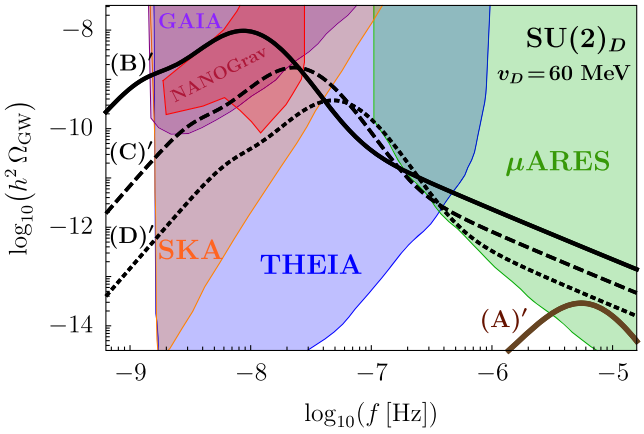

FIG. 5. Gravitational-wave signals arising from a first-order phase transition in the dark SU(2)$_D$ model [54] assuming $v_D = 60$ MeV, plotted for the Lagrangian parameters (g_D, λ) specified in Table II. The shaded regions correspond to the predicted sensitivity of future experiments, as explained in the caption of Fig. 3.

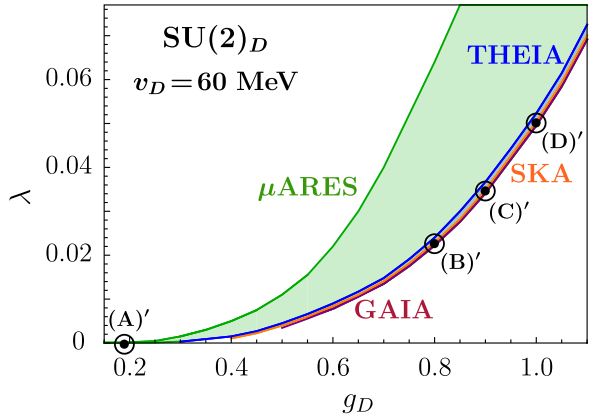

FIG. 6. Parameter space (g_D, λ) for which the gravitational-wave signal from a first-order phase transition in the dark SU(2)$_D$ model can be observed in future gravitational-wave and astrometry experiments, as explained in the caption of Fig. 4. The circled dots correspond to the signal curves shown in Fig. 5.

proposals THEIA [144] and GAIA [145,146]. In addition, we include the signal region suggested by the NANOGrav 15-year data [128].

As noted earlier, in our analysis we consider the entire parameter space of the U(1)$_D$ model, not just the region for which a neutron dark decay channel is kinematically available. Out of the four signals plotted in Fig. 3, only curve (A), which is equivalent to the benchmark point (A) given by Eq. (11), allows for the neutron dark decay channel $n \to \chi\phi$ to exist with a branching fraction of 1%.

The central peak of each of the signals is determined predominantly by the sound-wave contribution. The small bump visible on the left side of each spectrum is due to the bubble collision contribution, whereas the changes in slope on the right sides of the spectra is due to the magnetohydrodynamic turbulence contribution. We note that the sound-wave component would completely overwhelm the other contributions to the spectrum if not for the significant suppression coming from Υ in Eq. (40), reducing the signal by a factor of $\mathcal{O}(10\text{–}100)$. Our plots take into account this large suppression, without which the signals would be much stronger.

Table I specifies the first-order phase transition parameters: strength α, inverse of its duration $\tilde{\beta}$, and nucleation temperature T_*, corresponding to the Lagrangian parameters (g_D, λ) selected for the four signal curves. It also provides the masses of the scalar ϕ and dark photon A'. The peak frequency of the signal depends on the duration of the phase transition and the nucleation temperature, as described by Eq. (41); for faster phase transitions (larger $\tilde{\beta}$) and higher nucleation temperatures, the peak shifts to higher frequencies. Furthermore, the height of the peak is determined by the strength of the phase transition and its duration, resulting in a stronger signal for larger values of α and longer phase transitions, i.e., characterized by a smaller $\tilde{\beta}$.

A comment regarding the $\mathcal{O}(1\text{–}10)$ MeV nucleation temperatures is in place. In general, low values of T_* are tightly constrained by big bang nucleosynthesis and measurements of the cosmic microwave background radiation. A detailed analysis of the resulting bounds on the allowed nucleation temperatures for first-order phase transitions was carried out in [147,148]. Depending on the strength of the transition α, the lower limit on the nucleation temperature varies in the range $\mathcal{O}(1\text{–}2$ MeV). As seen from Table I, all of the points we selected satisfy these bounds.

To determine how much of the parameter space of the U(1)$_D$ model can be probed in gravitational-wave and astrometry experiments, we perform a scan over (g_D, λ). Figure 4 shows the regions of parameter space for the gauge coupling g_D versus the quartic coupling λ that give rise to signals detectable with a signal-to-noise ratio greater than 5 during the mission lifetime of GAIA (purple), THEIA (blue), SKA (orange), and μARES (green). For a given

TABLE II. Translation between the fundamental parameters (g_D, λ) of the SU(2)$_D$ model ($v_D = 60$ MeV) and the resulting phase transition parameters $(\alpha, \tilde{\beta}, T_*)$ for the signals plotted in Fig. 5.

	SU(2)$_D$ model parameters				Transition parameters		
Signal	g_D	λ	m_ϕ [MeV]	$m_{W'}$ [MeV]	α	$\tilde{\beta}$	T_* [MeV]
(A)′	0.19	0.0001	0.85	8	0.5	8700	3.3
(B)′	0.8	0.022	12.6	34	1.7	10	4.9
(C)′	0.9	0.034	15.6	38	0.8	20	6.7
(D)′	1.0	0.050	19.0	42	0.4	30	8.4

value of g_D, the larger the value of the quartic coupling λ, the weaker the signal and the higher the nucleation temperature. Thus, for each g_D the lower bound on λ corresponds to the lowest possible nucleation temperature for that value of g_D, and below this bound the value of $\mathcal{S}(T)/T$ is too large for Eq. (35) to be satisfied. The upper bound on λ arises from the limited sensitivity of an individual experiment. We note that all points in Fig. 4 fulfill the big bang nucleosynthesis and cosmic microwave background constraints discussed in [147,148]. Lowering the value of λ by too much for the benchmark point (A) (in order to strengthen the signal), although corresponding simply to choosing a smaller mass of ϕ, would lead to a lower nucleation temperature inconsistent with the discussed cosmological bounds. Therefore, the $\mathrm{U}(1)_D$ model with the neutron dark decay channel $n \to \chi\phi$ open can only be probed by the μARES experiment.

Quite remarkably, having chosen the vacuum expectation value $v_D = 60$ MeV that saturates the neutron star bound in Eq. (13), there exists a range of parameters for which the signal lies in the region of interest for the NANOGrav 15-year data result and which, at the same time, can be searched for in all other experiments considered here: GAIA, SKA, THEIA, and μARES. A detailed analysis of how well our signal fits the NANOGrav region is beyond the scope of this paper, especially since that case does not allow for the $n \to \chi\phi$ decay channel to exist. We refer the reader to the thorough model-independent analysis in [128].

Performing the same analysis as above for the dark $\mathrm{SU}(2)_D$ model, again keeping the vacuum expectation value fixed at $v_D = 60$ MeV, we obtain the gravitational-wave signals shown in Fig. 5. For an easier comparison with the previous case, three signal lines are chosen to correspond to the same values of the gauge coupling g_D as those in Fig. 3. The four signal curves in Fig. 5 correspond to the following parameter choices: $(g_D, \lambda) = (0.19, 0.0001)$ [brown solid line, curve $(\mathrm{A})'$], $(g_D, \lambda) = (0.8, 0.022)$ [black solid line, curve $(\mathrm{B})'$], $(g_D, \lambda) = (0.9, 0.034)$ [long-dashed line, curve $(\mathrm{C})'$], and $(g_D, \lambda) = (1.0, 0.050)$ [short-dashed line, curve (D')]. We overplot the predicted sensitivities of future gravitational-wave and astrometry experiments. Out of the four signals, only $(\mathrm{A})'$ corresponds to the scenario allowing for the decay channel $n \to \chi\phi$ to exist and it is equivalent to the benchmark point $(\mathrm{A})'$ given by Eq. (21); it can be searched for only with μARES.

Similarly as before, Table II specifies the first-order phase transition parameters $(\alpha, \tilde{\beta}, T_*)$, which correspond to the $\mathrm{SU}(2)_D$ model parameters (g_D, λ) for the four signal curves. The nucleation temperatures in this case are higher than for the $\mathrm{U}(1)_D$ model, and the discussed earlier lower bound on the nucleation temperature of $\mathcal{O}(1$–2 MeV) arising from cosmological measurements is again satisfied.

Upon performing a scan over the (g_D, λ) parameters of the model, we arrive at the results presented in Fig. 6, which shows the regions of parameter space for the gauge coupling g_D versus the quartic coupling λ giving rise to signals detectable with a signal-to-noise ratio greater than 5 during the mission lifetime of GAIA, THEIA, SKA, and μARES. It is evident that in this case higher values of the quartic coupling λ are required for the signal to be detectable. This is due to the fact that there are more degrees of freedom in the $\mathrm{SU}(2)_D$ model compared to the $\mathrm{U}(1)_D$ model, which strengthens the one-loop contribution to the effective potential, requiring a larger λ to balance this change.

VI. CONCLUSIONS

Recently, with the first successful direct detection of gravitational waves, particle physics acquired a new and extremely powerful tool to probe new physics models. Indeed, many extensions of the Standard Model are based on extra gauge symmetries at higher energy scales which, when spontaneously broken, may trigger a first-order phase transition, leading to the emission of a stochastic gravitational-wave background in the early Universe reaching us today. The shape of its spectrum is determined by the particle content of the model, thus providing insight into the high-energy structure of the theory. The literature on the subject is vast and predominantly models with symmetry-breaking scales beyond $\mathcal{O}(100$ GeV$)$ have been considered in this respect.

In this paper, we demonstrated that not only high-energy particle physics, but also low-energy physics such as nuclear physics, might benefit from the progress on the gravitational-wave front. We focused on models with a symmetry-breaking scale $\mathcal{O}(60$ MeV$)$ constructed to explain the neutron lifetime anomaly, which is a puzzling discrepancy between two different types of experiments measuring the neutron lifetime. These models, in certain regions of their parameter space, allow for the existence of a neutron dark decay channel with dark particles in the final state, with some being good dark matter candidates. We demonstrated that for a wide range of parameters, those models lead to a first-order phase transition in the early Universe, resulting in signatures that may be detectable in future experiments searching for gravitational waves at low frequencies.

In particular, we found that for a range of parameter values in the case of a model with a dark $\mathrm{U}(1)_D$ gauge group and a model with a dark $\mathrm{SU}(2)_D$ gauge group, the stochastic gravitational-wave background arising from a first-order phase transition in the early Universe falls within the reach of the future space-based gravitational-wave detector μARES, the pulsar timing array experiment SKA, and the planned astrometry experiments such as GAIA and THEIA. Since parts of the predicted gravitational-wave signals lie in regions of overlapping sensitivities of various detectors, this offers an opportunity of cross-checking the results, encouraging stronger

collaboration between the gravitational-wave and astrometry communities. Moreover, since the neutron dark decay proposal is currently being experimentally probed in various low-energy experiments, an opportunity of overlap also exists with the nuclear physics community.

In our analysis, we showed that, for both models considered, there exists a range of parameter values with the signal localized in the region corresponding to the lower portion of the recent NANOGrav 15-year data set region. It would be interesting to investigate, e.g., if an additional contribution from cosmic strings would produce a better fit to the upper part of the NANOGrav signal and, combined with the phase transition signal, could provide an explanation of the NANOGrav data. Such a cosmic string gravitational-wave signal can naturally arise from the breaking of the gauged lepton number $U(1)_\ell$ symmetry at high energies, which itself could lead to the seesaw mechanism for the neutrinos and constitute a natural extension of the models considered in this paper.

It goes without saying that a discovery of any primordial gravitational-wave background would lead to a much needed breakthrough in particle physics. What makes the models considered in this paper special is that they can be probed by many different experiments, leading to multiple synergies between physics disciplines, which seems to be the most promising way forward in our quest to discover the truth about the dark side of the Universe.

ACKNOWLEDGMENTS

This research was supported by the National Science Foundation under Grant No. PHY-2213144.

[1] S. L. Glashow, Partial symmetries of weak interactions, Nucl. Phys. **22**, 579 (1961).
[2] P. W. Higgs, Broken symmetries and the masses of gauge bosons, Phys. Rev. Lett. **13**, 508 (1964).
[3] F. Englert and R. Brout, Broken symmetry and the mass of gauge vector mesons, Phys. Rev. Lett. **13**, 321 (1964).
[4] S. Weinberg, A model of leptons, Phys. Rev. Lett. **19**, 1264 (1967).
[5] A. Salam, Weak and electromagnetic interactions, Conf. Proc. **C1680519**, 367 (1968).
[6] H. Fritzsch, M. Gell-Mann, and H. Leutwyler, Advantages of the color octet gluon picture, Phys. Lett. **47B**, 365 (1973).
[7] D. J. Gross and F. Wilczek, Ultraviolet behavior of non-abelian gauge theories, Phys. Rev. Lett. **30**, 1343 (1973).
[8] H. D. Politzer, Reliable perturbative results for strong interactions?, Phys. Rev. Lett. **30**, 1346 (1973).
[9] S. Chatrchyan *et al.* (CMS Collaboration), Observation of a new boson at a mass of 125 GeV with the CMS experiment at the LHC, Phys. Lett. B **716**, 30 (2012).
[10] G. Aad *et al.* (ATLAS Collaboration), Observation of a new particle in the search for the standard model Higgs boson with the ATLAS detector at the LHC, Phys. Lett. B **716**, 1 (2012).
[11] V. C. Rubin and W. K. Ford, Jr., Rotation of the Andromeda nebula from a spectroscopic survey of emission regions, Astrophys. J. **159**, 379 (1970).
[12] P. de Bernardis *et al.* (Boomerang Collaboration), A flat universe from high resolution maps of the cosmic microwave background radiation, Nature (London) **404**, 955 (2000).
[13] R. Gavazzi, T. Treu, J. D. Rhodes, L. V. Koopmans, A. S. Bolton, S. Burles, R. Massey, and L. A. Moustakas, The sloan lens ACS survey. 4. The mass density profile of early-type galaxies out to 100 effective radii, Astrophys. J. **667**, 176 (2007).
[14] W. H. Press, B. S. Ryden, and D. N. Spergel, Single mechanism for generating large scale structure and providing dark missing matter, Phys. Rev. Lett. **64**, 1084 (1990).
[15] L. Hui, J. P. Ostriker, S. Tremaine, and E. Witten, Ultralight scalars as cosmological dark matter, Phys. Rev. D **95**, 043541 (2017).
[16] E. W. Kolb, D. J. H. Chung, and A. Riotto, WIMPzillas!, AIP Conf. Proc. **484**, 91 (1999).
[17] K. A. Meissner and H. Nicolai, Planck mass charged gravitino dark matter, Phys. Rev. D **100**, 035001 (2019).
[18] J. L. Feng, Dark matter candidates from particle physics and methods of detection, Annu. Rev. Astron. Astrophys. **48**, 495 (2010).
[19] Y. Bai, A. J. Long, and S. Lu, Dark quark nuggets, Phys. Rev. D **99**, 055047 (2019).
[20] B. J. Carr, K. Kohri, Y. Sendouda, and J. Yokoyama, New cosmological constraints on primordial black holes, Phys. Rev. D **81**, 104019 (2010).
[21] S. Bird, I. Cholis, J. B. Munoz, Y. Ali-Haimoud, M. Kamionkowski, E. D. Kovetz, A. Raccanelli, and A. G. Riess, Did LIGO detect dark matter?, Phys. Rev. Lett. **116**, 201301 (2016).
[22] E. Aprile *et al.* (XENON Collaboration), Physics reach of the XENON1T dark matter experiment, J. Cosmol. Astropart. Phys. 04 (2016) 027.
[23] M. Ackermann *et al.* (Fermi-LAT Collaboration), The Fermi Galactic center GeV excess and implications for dark matter, Astrophys. J. **840**, 43 (2017).
[24] S. Nussinov, Technocosmology? Could a technibaryon excess provide a natural missing mass candidate?, Phys. Lett. **165B**, 55 (1985).
[25] D. B. Kaplan, A single explanation for both the baryon and dark matter densities, Phys. Rev. Lett. **68**, 741 (1992).
[26] D. Hooper, J. March-Russell, and Stephen M. West, Asymmetric sneutrino dark matter and the $\Omega_b/\Omega_{\rm DM}$ puzzle, Phys. Lett. B **605**, 228 (2005).

[27] D. E. Kaplan, M. A. Luty, and K. M. Zurek, Asymmetric dark matter, Phys. Rev. D **79**, 115016 (2009).
[28] K. Petraki and R. R. Volkas, Review of asymmetric dark matter, Int. J. Mod. Phys. A **28**, 1330028 (2013).
[29] K. M. Zurek, Asymmetric dark matter: Theories, signatures, and constraints, Phys. Rep. **537**, 91 (2014).
[30] B. Fornal and B. Grinstein, Dark matter interpretation of the neutron decay anomaly, Phys. Rev. Lett. **120**, 191801 (2018); **124**, 219901(E) (2020).
[31] A. Serebrov *et al.*, Measurement of the neutron lifetime using a gravitational trap and a low-temperature fomblin coating, Phys. Lett. B **605**, 72 (2005).
[32] A. Pichlmaier, V. Varlamov, K. Schreckenbach, and P. Geltenbort, Neutron lifetime measurement with the UCN trap-in-trap MAMBO II, Phys. Lett. B **693**, 221 (2010).
[33] A. Steyerl, J. M. Pendlebury, C. Kaufman, S. S. Malik, and A. M. Desai, Quasielastic scattering in the interaction of ultracold neutrons with a liquid wall and application in a reanalysis of the Mambo I neutron lifetime experiment, Phys. Rev. C **85**, 065503 (2012).
[34] S. Arzumanov, L. Bondarenko, S. Chernyavsky, P. Geltenbort, V. Morozov, V. V. Nesvizhevsky, Yu. Panin, and A. Strepetov, A measurement of the neutron lifetime using the method of storage of ultracold neutrons and detection of inelastically up-scattered neutrons, Phys. Lett. B **745**, 79 (2015).
[35] A. P. Serebrov *et al.*, Neutron lifetime measurements with a large gravitational trap for ultracold neutrons, Phys. Rev. C **97**, 055503 (2018).
[36] R. W. Pattie, Jr. *et al.*, Measurement of the neutron lifetime using a magneto-gravitational trap and *in situ* detection, Science **360**, 627 (2018).
[37] V. F. Ezhov *et al.*, Measurement of the neutron lifetime with ultra-cold neutrons stored in a magneto-gravitational trap, JETP Lett. **107**, 671 (2018).
[38] F. M. Gonzalez *et al.* (UCNτ Collaboration), Improved neutron lifetime measurement with UCNτ, Phys. Rev. Lett. **127**, 162501 (2021).
[39] J. Byrne and P. G. Dawber, A revised value for the neutron lifetime measured using a penning trap, Europhys. Lett. **33**, 187 (1996).
[40] J. S. Nico *et al.*, Measurement of the neutron lifetime by counting trapped protons in a cold neutron beam, Phys. Rev. C **71**, 055502 (2005).
[41] A. T. Yue, M. S. Dewey, D. M. Gilliam, G. L. Greene, A. B. Laptev, J. S. Nico, W. M. Snow, and F. E. Wietfeldt, Improved determination of the neutron lifetime, Phys. Rev. Lett. **111**, 222501 (2013).
[42] K. Hirota *et al.*, Neutron lifetime measurement with pulsed cold neutrons, Prog. Theor. Exp. Phys. **2020**, 123C02 (2020).
[43] G. Baym, D. H. Beck, P. Geltenbort, and J. Shelton, Testing dark decays of baryons in neutron stars, Phys. Rev. Lett. **121**, 061801 (2018).
[44] D. McKeen, A. E. Nelson, S. Reddy, and D. Zhou, Neutron stars exclude light dark baryons, Phys. Rev. Lett. **121**, 061802 (2018).
[45] T. F. Motta, P. A. M. Guichon, and A. W. Thomas, Implications of neutron star properties for the existence of light dark matter, J. Phys. G **45**, 05LT01 (2018).
[46] D. Barducci, M. Fabbrichesi, and E. Gabrielli, Neutral hadrons disappearing into the darkness, Phys. Rev. D **98**, 035049 (2018).
[47] B. Grinstein, C. Kouvaris, and N. G. Nielsen, Neutron star stability in light of the neutron decay anomaly, Phys. Rev. Lett. **123**, 091601 (2019).
[48] J. M. Cline and J. M. Cornell, Dark decay of the neutron, J. High Energy Phys. 07 (2018) 081.
[49] G. K. Karananas and A. Kassiteridis, Small-scale structure from neutron dark decay, J. Cosmol. Astropart. Phys. 09 (2018) 036.
[50] T. Bringmann, J. M. Cline, and J. M. Cornell, Baryogenesis from neutron–dark matter oscillations, Phys. Rev. D **99**, 035024 (2019).
[51] Z. Berezhiani, Neutron lifetime puzzle and neutron–mirror neutron oscillation, Eur. Phys. J. C **79**, 484 (2019).
[52] M. Jin and Y. Gao, Nucleon—light dark matter annihilation through baryon number violation, Phys. Rev. D **98**, 075026 (2018).
[53] W.-Y. Keung, D. Marfatia, and P.-Y. Tseng, Annihilation signatures of neutron dark decay models in neutron oscillation and proton decay searches, J. High Energy Phys. 09 (2019) 053.
[54] F. Elahi and M. Mohammadi Najafabadi, Neutron decay to a non-Abelian dark sector, Phys. Rev. D **102**, 035011 (2020).
[55] B. Fornal, B. Grinstein, and Y. Zhao, Dark matter capture by atomic nuclei, Phys. Lett. B **811**, 135869 (2020).
[56] D. McKeen and M. Pospelov, How long does the hydrogen atom live?, Universe **9**, 473 (2023).
[57] G. Alonso-Alvarez, G. Elor, M. Escudero, B. Fornal, B. Grinstein, and J. Martin Camalich, Strange physics of dark baryons, Phys. Rev. D **105**, 115005 (2022).
[58] Z. Tang *et al.*, Search for the neutron decay $n \to X + \gamma$ where X is a dark matter particle, Phys. Rev. Lett. **121**, 022505 (2018).
[59] X. Sun *et al.* (UCNA Collaboration), Search for dark matter decay of the free neutron from the UCNA experiment: $n \to \chi + e^+e^-$, Phys. Rev. C **97**, 052501 (2018).
[60] M. Pfutzner and K. Riisager, Examining the possibility to observe neutron dark decay in nuclei, Phys. Rev. C **97**, 042501 (2018).
[61] M. Klopf, E. Jericha, B. Markisch, H. Saul, T. Soldner, and H. Abele, Constraints on the dark matter interpretation $n \to \chi + e^+e^-$ of the neutron decay anomaly with the PERKEO II experiment, Phys. Rev. Lett. **122**, 222503 (2019).
[62] Y. Ayyad *et al.*, Direct observation of proton emission in ^{11}Be, Phys. Rev. Lett. **123**, 082501 (2019); **124**, 129902(E) (2020).
[63] Y. Ayyad *et al.*, Evidence of a near-threshold resonance in ^{11}Be relevant to the β-delayed proton emission of ^{11}Be, Phys. Rev. Lett. **129**, 012501 (2022).
[64] E. Lopez-Saavedra *et al.*, Observation of a near-threshold proton resonance in ^{11}Be, Phys. Rev. Lett. **129**, 012502 (2022).
[65] Z. Tang *et al.*, Ultra-cold Neutron measurement of Proton branching ratio in neutron beta decay (UCNProBe), in Talk at the APS April Meeting 2019 (Denver, CO, 2019), https://meetings.aps.org/Meeting/APR19/Session/H14.5.

[66] M. Hassan, N. Floyd, Z. Tang, and UCNProBe Team, The current status of the UCNProBe experiment, in *APS Division of Nuclear Physics Meeting Abstracts, APS Meeting Abstracts* Vol. 2021 (2021), p. QJ.008, https://ui.adsabs.harvard.edu/abs/2021APS..DNP.QJ008H/abstract.
[67] B. Fornal, Neutron dark decay, Universe **9**, 449 (2023).
[68] B. P. Abbott *et al.* (LIGO Scientific and Virgo Collaborations), Observation of gravitational waves from a binary black hole merger, Phys. Rev. Lett. **116**, 061102 (2016).
[69] A. Kosowsky, M. S. Turner, and R. Watkins, Gravitational radiation from colliding vacuum bubbles, Phys. Rev. D **45**, 4514 (1992).
[70] T. Vachaspati and A. Vilenkin, Gravitational radiation from cosmic strings, Phys. Rev. D **31**, 3052 (1985).
[71] M. Sakellariadou, Gravitational waves emitted from infinite strings, Phys. Rev. D **42**, 354 (1990); **43**, 4150(E) (1991).
[72] T. Hiramatsu, M. Kawasaki, and K. Saikawa, Gravitational waves from collapsing domain walls, J. Cosmol. Astropart. Phys. 05 (2010) 032.
[73] M. S. Turner, Detectability of inflation produced gravitational waves, Phys. Rev. D **55**, R435 (1997).
[74] C. Grojean and G. Servant, Gravitational waves from phase transitions at the electroweak scale and beyond, Phys. Rev. D **75**, 043507 (2007).
[75] V. Vaskonen, Electroweak baryogenesis and gravitational waves from a real scalar singlet, Phys. Rev. D **95**, 123515 (2017).
[76] G. C. Dorsch, S. J. Huber, T. Konstandin, and J. M. No, A second Higgs doublet in the early universe: Baryogenesis and gravitational waves, J. Cosmol. Astropart. Phys. 05 (2017) 052.
[77] J. Bernon, L. Bian, and Y. Jiang, A new insight into the phase transition in the early universe with two Higgs doublets, J. High Energy Phys. 05 (2018) 151.
[78] I. Baldes and G. Servant, High scale electroweak phase transition: Baryogenesis and symmetry non-restoration, J. High Energy Phys. 10 (2018) 053.
[79] M. Chala, C. Krause, and G. Nardini, Signals of the electroweak phase transition at colliders and gravitational wave observatories, J. High Energy Phys. 07 (2018) 062.
[80] A. Alves, T. Ghosh, H.-K. Guo, K. Sinha, and D. Vagie, Collider and gravitational wave complementarity in exploring the singlet extension of the standard model, J. High Energy Phys. 04 (2019) 052.
[81] X.-F. Han, L. Wang, and Y. Zhang, Dark matter electroweak phase transition, and gravitational waves in the type II two-Higgs-doublet model with a singlet scalar field, Phys. Rev. D **103**, 035012 (2021).
[82] F. Costa, S. Khan, and J. Kim, A two-component dark matter model and its associated gravitational waves, J. High Energy Phys. 06 (2022) 026.
[83] P. Schwaller, Gravitational waves from a dark phase transition, Phys. Rev. Lett. **115**, 181101 (2015).
[84] I. Baldes, Gravitational waves from the asymmetric-dark-matter generating phase transition, J. Cosmol. Astropart. Phys. 05 (2017) 028.
[85] M. Breitbach, J. Kopp, E. Madge, T. Opferkuch, and P. Schwaller, Dark, cold, and noisy: Constraining secluded hidden sectors with gravitational waves, J. Cosmol. Astropart. Phys. 07 (2019) 007.
[86] D. Croon, V. Sanz, and G. White, Model discrimination in gravitational wave spectra from dark phase transitions, J. High Energy Phys. 08 (2018) 203.
[87] E. Hall, T. Konstandin, R. McGehee, H. Murayama, and G. Servant, Baryogenesis from a dark first-order phase transition, J. High Energy Phys. 04 (2020) 042.
[88] B. Fornal and E. Pierre, Asymmetric dark matter from gravitational waves, Phys. Rev. D **106**, 115040 (2022).
[89] M. Kierkla, A. Karam, and B. Swiezewska, Conformal model for gravitational waves and dark matter: A status update, J. High Energy Phys. 03 (2023) 007.
[90] F. Costa, S. Khan, and J. Kim, A two-component vector WIMP—Fermion FIMP dark matter model with an extended seesaw mechanism, J. High Energy Phys. 12 (2022) 165.
[91] P. S. B. Dev, F. Ferrer, Y. Zhang, and Y. Zhang, Gravitational waves from first-order phase transition in a simple axion-like particle model, J. Cosmol. Astropart. Phys. 11 (2019) 006.
[92] B. Von Harling, A. Pomarol, O. Pujolas, and F. Rompineve, Peccei-Quinn phase transition at LIGO, J. High Energy Phys. 04 (2020) 195.
[93] L. Delle Rose, G. Panico, M. Redi, and A. Tesi, Gravitational waves from supercool axions, J. High Energy Phys. 04 (2020) 025.
[94] R. Z. Ferreira, A. Notari, O. Pujolas, and F. Rompineve, High quality QCD axion at gravitational wave observatories, Phys. Rev. Lett. **128**, 141101 (2022).
[95] D. Croon, T. E. Gonzalo, and G. White, Gravitational waves from a Pati-Salam phase transition, J. High Energy Phys. 02 (2019) 083.
[96] W.-C. Huang, F. Sannino, and Z.-W. Wang, Gravitational waves from Pati-Salam dynamics, Phys. Rev. D **102**, 095025 (2020).
[97] N. Okada, O. Seto, and H. Uchida, Gravitational waves from breaking of an extra $U(1)$ in $SO(10)$ grand unification, Prog. Theor. Exp. Phys. **2021**, 033B01 (2021).
[98] B. Fornal, K. Garcia, and E. Pierre, Testing unification and dark matter with gravitational waves, Phys. Rev. D **108**, 055022 (2023).
[99] J. Ellis, M. Lewicki, and V. Vaskonen, Updated predictions for gravitational waves produced in a strongly supercooled phase transition, J. Cosmol. Astropart. Phys. 11 (2020) 020.
[100] K. Kawana, Cosmology of a supercooled universe, Phys. Rev. D **105**, 103515 (2022).
[101] N. Craig, N. Levi, A. Mariotti, and D. Redigolo, Ripples in spacetime from broken supersymmetry, J. High Energy Phys. 02 (2020) 184.
[102] B. Fornal, B. Shams Es Haghi, J.-H. Yu, and Y. Zhao, Gravitational waves from mini-split SUSY, Phys. Rev. D **104**, 115005 (2021).
[103] V. Brdar, L. Graf, A. J. Helmboldt, and X.-J. Xu, Gravitational waves as a probe of left-right symmetry breaking, J. Cosmol. Astropart. Phys. 12 (2019) 027.
[104] L. Graf, S. Jana, A. Kaladharan, and S. Saad, Gravitational wave imprints of left-right symmetric model with minimal Higgs sector, J. Cosmol. Astropart. Phys. 05 (2022) 003.

[105] V. Brdar, A. J. Helmboldt, and J. Kubo, Gravitational waves from first-order phase transitions: LIGO as a window to unexplored seesaw scales, J. Cosmol. Astropart. Phys. 02 (2019) 021.
[106] N. Okada and O. Seto, Probing the seesaw scale with gravitational waves, Phys. Rev. D **98**, 063532 (2018).
[107] P. Di Bari, D. Marfatia, and Y.-L. Zhou, Gravitational waves from first-order phase transitions in Majoron models of neutrino mass, J. High Energy Phys. 10 (2021) 193.
[108] R. Zhou, L. Bian, and Y. Du, Electroweak phase transition and gravitational waves in the type-II seesaw model, J. High Energy Phys. 08 (2022) 205.
[109] T. Hasegawa, N. Okada, and O. Seto, Gravitational waves from the minimal gauged $U(1)_{B-L}$ model, Phys. Rev. D **99**, 095039 (2019).
[110] B. Fornal and B. Shams Es Haghi, Baryon and lepton number violation from gravitational waves, Phys. Rev. D **102**, 115037 (2020).
[111] J. Bosch, Z. Delgado, B. Fornal, and A. Leon, Gravitational wave signatures of gauged baryon and lepton number, Phys. Rev. D **108**, 095014 (2023).
[112] A. Greljo, T. Opferkuch, and B. A. Stefanek, Gravitational imprints of flavor hierarchies, Phys. Rev. Lett. **124**, 171802 (2020).
[113] B. Fornal, Gravitational wave signatures of lepton universality violation, Phys. Rev. D **103**, 015018 (2021).
[114] A. Dasgupta, P. S. B. Dev, A. Ghoshal, and A. Mazumdar, Gravitational wave pathway to testable leptogenesis, Phys. Rev. D **106**, 075027 (2022).
[115] E. J. Chun, T. P. Dutka, T. H. Jung, X. Nagels, and M. Vanvlasselaer, Bubble-assisted leptogenesis, J. High Energy Phys. 09 (2023) 164.
[116] R. Caldwell *et al.*, Detection of early-universe gravitational-wave signatures and fundamental physics, Gen. Relativ. Gravit. **54**, 156 (2022).
[117] C. Badger, B. Fornal, K. Martinovic, A. Romero, K. Turbang, H. Guo, A. Mariotti, M. Sakellariadou, A. Sevrin, F.-W. Yang, and Y. Zhao, Probing early universe supercooled phase transitions with gravitational wave data, Phys. Rev. D **107**, 023511 (2023).
[118] P. Amaro-Seoane *et al.* (LISA Collaboration), Laser interferometer space antenna, arXiv:1702.00786.
[119] D. Reitze *et al.*, Cosmic Explorer: The U.S. contribution to gravitational-wave astronomy beyond LIGO, Bull. Am. Astron. Soc. **51**, 035 (2019), https://baas.aas.org/pub/2020n7i035/release/1.
[120] J. Crowder and N. J. Cornish, Beyond LISA: Exploring future gravitational wave missions, Phys. Rev. D **72**, 083005 (2005).
[121] M. Punturo *et al.*, The Einstein Telescope: A third-generation gravitational wave observatory, Classical Quantum Gravity **27**, 194002 (2010).
[122] S. Kawamura *et al.*, The Japanese space gravitational wave antenna: DECIGO, Classical Quantum Gravity **28**, 094011 (2011).
[123] Z. Arzoumanian *et al.* (NANOGRAV Collaboration), The NANOGrav 11-year data set: Pulsar-timing constraints on the stochastic gravitational-wave background, Astrophys. J. **859**, 47 (2018).
[124] R. N. Manchester *et al.*, The parkes pulsar timing array project, Publ. Astron. Soc. Aust. **30**, e017 (2013).
[125] R. D. Ferdman *et al.*, The European pulsar timing array: Current efforts and a LEAP toward the future, Classical Quantum Gravity **27**, 084014 (2010).
[126] G. Hobbs *et al.*, The international pulsar timing array project: Using pulsars as a gravitational wave detector, Classical Quantum Gravity **27**, 084013 (2010).
[127] A. Weltman *et al.*, Fundamental physics with the square kilometre array, Publ. Astron. Soc. Aust. **37**, e002 (2020).
[128] A. Afzal *et al.* (NANOGrav Collaboration), The NANOGrav 15 yr data set: Search for signals from new physics, Astrophys. J. Lett. **951**, L11 (2023).
[129] Y. Aoki, T. Izubuchi, E. Shintani, and A. Soni, Improved lattice computation of proton decay matrix elements, Phys. Rev. D **96**, 014506 (2017).
[130] G. W. Anderson and L. J. Hall, The electroweak phase transition and baryogenesis, Phys. Rev. D **45**, 2685 (1992).
[131] M. Quiros, Field theory at finite temperature and phase transitions, Acta Phys. Pol. B **38**, 3661 (2007), https://www.actaphys.uj.edu.pl/R/38/12/3661/pdf.
[132] D. Comelli and J. R. Espinosa, Bosonic thermal masses in supersymmetry, Phys. Rev. D **55**, 6253 (1997).
[133] A. D. Linde, Decay of the false vacuum at finite temperature, Nucl. Phys. **B216**, 421 (1983).
[134] J. R. Espinosa, T. Konstandin, J. M. No, and G. Servant, Energy budget of cosmological first-order phase transitions, J. Cosmol. Astropart. Phys. 06 (2010) 028.
[135] C. Caprini *et al.*, Science with the space-based interferometer eLISA. II: Gravitational waves from cosmological phase transitions, J. Cosmol. Astropart. Phys. 04 (2016) 001.
[136] M. Hindmarsh, S. J. Huber, K. Rummukainen, and D. J. Weir, Gravitational waves from the sound of a first order phase transition, Phys. Rev. Lett. **112**, 041301 (2014).
[137] J. Ellis, M. Lewicki, and J. M. No, Gravitational waves from first-order cosmological phase transitions: Lifetime of the sound wave source, J. Cosmol. Astropart. Phys. 07 (2020) 050.
[138] H.-K. Guo, K. Sinha, D. Vagie, and G. White, Phase transitions in an expanding universe: Stochastic gravitational waves in standard and non-standard histories, J. Cosmol. Astropart. Phys. 01 (2021) 001.
[139] S. J. Huber and T. Konstandin, Gravitational wave production by collisions: More bubbles, J. Cosmol. Astropart. Phys. 09 (2008) 022.
[140] M. Kamionkowski, A. Kosowsky, and M. S. Turner, Gravitational radiation from first order phase transitions, Phys. Rev. D **49**, 2837 (1994).
[141] C. Caprini and R. Durrer, Gravitational waves from stochastic relativistic sources: Primordial turbulence and magnetic fields, Phys. Rev. D **74**, 063521 (2006).
[142] C. Caprini, R. Durrer, and G. Servant, The stochastic gravitational wave background from turbulence and magnetic fields generated by a first-order phase transition, J. Cosmol. Astropart. Phys. 12 (2009) 024.
[143] A. Sesana *et al.*, Unveiling the gravitational universe at μ-Hz frequencies, Exp. Astron. **51**, 1333 (2021).

[144] J. Garcia-Bellido, H. Murayama, and G. White, Exploring the early universe with GAIA and THEIA, J. Cosmol. Astropart. Phys. 12 (2021) 023.

[145] A. G. A. Brown *et al.* (Gaia Collaboration), Gaia data release 2. Summary of the contents and survey properties, Astron. Astrophys. **616**, A1 (2018).

[146] C. J. Moore, D. P. Mihaylov, A. Lasenby, and G. Gilmore, Astrometric search method for individually resolvable gravitational wave sources with gaia, Phys. Rev. Lett. **119**, 261102 (2017).

[147] Y. Bai and M. Korwar, Cosmological constraints on first-order phase transitions, Phys. Rev. D **105**, 095015 (2022).

[148] S. Deng and L. Bian, Constraints on new physics around the MeV scale with cosmological observations, Phys. Rev. D **108**, 063516 (2023).